The Effect of Atmosphere and ZnO Morphology on the Performance of Hybrid Poly(3-hexylthiophene)/ZnO Nanofiber Photovoltaic Devices

ARTICLE *in* THE JOURNAL OF PHYSICAL CHEMISTRY C · OCTOBER 2007

Impact Factor: 4.77 · DOI: 10.1021/jp0734225

The Effect of Atmosphere and ZnO Morphology on the Performance of Hybrid Poly(3-hexylthiophene)/ZnO Nanofiber Photovoltaic Devices

Dana C. Olson,[†,‡] Sean E. Shaheen,[†] Reuben T. Collins,[‡] and David S. Ginley*[,†]

National Renewable Energy Laboratory, Golden, Colorado 80401, and Department of Physics, Colorado School of Mines, Golden, Colorado 80401

Received: May 4, 2007; In Final Form: July 16, 2007

We present detailed investigations of the fabrication and characterization of photovoltaic devices consisting of poly(3-hexylthiophene) (P3HT) intercalated into a mesoporous structure of ZnO nanofibers. ZnO nanofibers were grown via a low-temperature hydrothermal route from a solution of zinc nitrate precursor. P3HT was spin-coated on top of the structure, and intercalation into the voids between the nanofibers was induced with annealing. A silver electrode was used as the top contact. Spin-coating, storage, and testing of the device were performed in air. We discuss the effects of atmosphere and ZnO nanofiber morphology on device performance. Optimized nanofiber devices exhibited a 4-fold increase in the short circuit current (2.17 mA/cm^2) as compared to that of a planar ZnO−P3HT bilayer device (0.52 mA/cm^2) as a result of the increased donor−acceptor interfacial area. The efficiency of the nanofiber based device under 1 sun-simulated solar illumination was 0.53% and was found to increase at higher incident light intensities, reaching a value of 0.61% at 2.5 suns. Additionally, we found that for these devices fabrication in and exposure to air is required to obtain good diode characteristics. We also show that the morphology of the ZnO nanostructures in the nanocomposite directly impacts device performance. Treatment of the ZnO surface using surfactants increased the open circuit voltage at the expense of the short circuit current; however, there was little effect on overall device efficiency. Because of the inverted geometry of this device that allowed for the use of a silver top contact, the device was not susceptible to oxidative degradation when stored in the dark.

Introduction

Organic-based photovoltaics (OPV) offer the promise to serve as a low cost, large area alternative to conventional photovoltaics.[1] Ideally, all of the steps in the device fabrication would be done using atmospheric, low-temperature, solution-based processing allowing for the use of plastic substrates. A number of OPV device approaches have been demonstrated to date, with several reports of certified AM 1.5 power conversion efficiencies greater than 5% for polymer-fullerene blend devices.[2−5] A key factor in OPV device design and performance is the careful control of morphology, leading to efficient dissociation of all generated excitons, and subsequent transport of charge carriers out of the device. Present donor−acceptor blend devices rely largely on morphological control through solvent selection and annealing processes,[6] which otherwise result in disordered material structures that can lead to increased recombination, reduced carrier mobilities, and low power conversion efficiencies.

Excitons in polymer/fullerene blend devices are dissociated through the photoinduced charge transfer between the electron donor poly(3-hexylthiophene) (P3HT) and the acceptor (6,6)-phenyl C61 butyric acid methyl ester (PCBM). Many groups have shown that photoinduced charge transfer can also occur between a conjugated polymer and a metal oxide semiconductor such as SnO_2, TiO_2, or ZnO.[7−9] One approach for a hybrid polymer/inorganic device uses blends of oxide semiconductor nanoparticles embedded in a conjugated polymer matrix.[10,11] These devices presently suffer from incomplete exciton dissociation due to nonideal dispersion of the nanoparticles in the blend and low carrier mobility through the nanoparticle pathways in the blend. Similar hybrid devices have been prepared from metal oxide precursors and conjugated polymers, where the metal oxide precursor is transformed after the composite film has formed resulting in a metal oxide/conjugated polymer composite device.[9,12] It was shown that ZnO nanoparticles demonstrated better performance than TiO_2 nanoparticles; however, these devices are still limited by incomplete exciton dissociation and the polycrystalline nature of the metal oxide. In another approach, bulk heterojunction devices based on a blend of P3HT with CdSe nanoparticles have demonstrated the advantage of CdSe nanorods over spherical particles, resulting in enhanced photovoltaic performance through improved transport and increased absorption through the use of two absorbing materials.[13] However, the electron mobility in polymer blends with CdSe nanoparticles is still quite low at 10^{-6} cm^2 v^{-1} s^{-1}, which may limit efficiency.[14] These studies have demonstrated the feasibility of the hybrid approach, although the morphologies of the nanostructured inorganic semiconductors have not been ideal, and reported device efficiencies have not exceeded 2%.

The devices in this work are based on infiltrating conjugated polymers into a mesoporous, nanostructured oxide semiconductor networks. This approach has demonstrated directed control of the morphology of the heterojunction interface.[15−20] The reported efficiencies in these devices are presently limited due to the disordered nature of the polymer in the very small pores

* To whom correspondence should be addressed.
† National Renewable Energy Laboratory.
‡ Colorado School of Mines.

10.1021/jp0734225 CCC: $37.00
Published on Web 10/10/2007

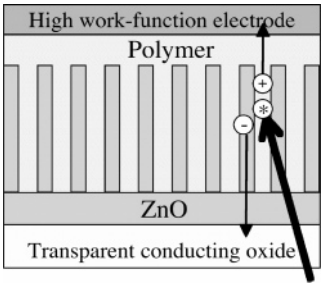

Figure 1. Schematic diagram of an ideal nanostructured oxide/conjugated polymer photovoltaic device.

in the polycrystalline metal oxide and to the quality of the interfaces between the inorganic and organic materials.

A nanostructured oxide that is vertically aligned with respect to the substrate offers a promising means to increase the efficiencies of these devices. ZnO is a good candidate for this application as preferential growth of single-crystal ZnO fibers from a nucleation layer has been demonstrated to be in the (001) direction, normal to the substrate. This increases the donor−acceptor interfacial area and creates high mobility electron transport pathways connected only to the negative electrode. For instance, the electron mobility of ZnO has been measured to be as high as 400 $cm^2\ V^{-1}\ s^{-1}$ for pulse laser deposited thin films[21,22] and >20 $cm^2\ V^{-1}\ s^{-1}$ in ZnO nanofibers,[23,24] which are several orders of magnitude higher than what is typically found in organic semiconductors. Dye-sensitized solar cells have been fabricated using ZnO nanowire anodes with efficiencies greater than 1.5% and have demonstrated improved electron transport and electron injection in single-crystal nanowires over polycrystalline networks of sintered ZnO nanoparticle films.[24] A schematic of a composite device based on vertically aligned nanostructures is presented in Figure 1.

In this device architecture, nanofibers are first grown vertically off the substrate using a chemical solution growth technique to produce a nanostructured oxide. The surface of the oxide may then be coated with an interface modifier. Intercalation of conjugated polymer is then done by, for instance, spin-coating the polymer onto the top surface of the oxide, followed by an annealing step to induce filling of the porous volume of the oxide. Finally, a top contact is deposited onto the conjugated polymer.

Materials and Methods

Materials. The P3HT was used as received from Merck. The weight-averaged molecular weight of the P3HT was 21 000 g/mol. Zinc acetate (ZnAc) and zinc nitrate were used as received from the Sigma-Aldrich Company.

Device Fabrication. Devices were fabricated on patterned indium tin oxide (ITO)-coated glass substrates with a sheet resistance of 13 Ω/cm^2 that were first cleaned by ultrasonic agitation in acetone, chloroform, and isopropanol for 10 min each followed by an oxygen plasma treatment of 150 W at 500 mTorr for 5 min. A nucleation layer of ZnO was spin-coated onto the ITO, which functions as the transparent negative electrode, using a zinc acetate−ethanol amine solution in 2-methoxyethanol, where the ratio of ethanol amine to ZnAc was 1.0 and the concentration of ZnAc was 0.75 M.[25] After thermal annealing the ZnAc film for 5 min at 300 °C in air, the ZnO film is rinsed with deionized water and ethanol. Next, ZnO nanofibers were hydrothermally grown from the nucleation layer in a 1 mM solution of zinc nitrate in deionized water adjusted to pH 13 with NaOH for 20 min at 70 °C.[26,27] The sample was rinsed again and then dried in air for 10 min at 200 °C. For the ZnO fiber/P3HT device, a 200 nm layer of P3HT is then spin-coated from a 30 mg/mL chloroform solution on top of this structure, followed by another thermal anneal at 200 °C for 1 min under an argon atmosphere. A 100 nm silver top contact was deposited via thermal evaporation through a shadow mask to form the positive back electrode with active areas for each device of 0.1 cm^2. Bilayer devices were fabricated in the same manner; however, the ZnO fiber growth was omitted from the process. Devices were subsequently stored in air in the dark.

In this inverted geometry, the back electrode is the positive contact and therefore must be a high work function metal to form an ohmic contact to the polymer. Silver is used as the anode, as it has led to the highest performance compared to either gold or palladium. Silver has been used successfully in similar device architectures[18] and has been observed to coordinate with the sulfur atom in the thiophene.[28] Additionally, a shift in the band alignment of the metal/organic interface has been observed in Ag/porphyrin, where the work function increases by 0.7 eV upon exposure to oxygen; it is expected that a similar effect is observed here. Thus, the silver actually functions as a high work-function silver oxide electrode in these devices.

Optical and Structural Measurements. Scanning electron microscopy (SEM) images were recorded on a JEOL 6320 FE-SEM. X-ray diffraction (XRD) data were performed on a Bruker equip with a two-dimensional large area detector and an *x-y* sample positioning stage. Profilometry was done using a Dektak 3 profilometer. Absorption spectra were recorded on a Hewlett-Packard 8453 UV−vis spectrophotometer. Photoluminescence (PL) spectra were taken on a SPEX Fluorolog with a Xenon arc lamp. Samples were pumped with light at 275 nm and were integrated for 1 s with a step size of 1 nm.

Electrical Measurements. All photovoltaic characterizations were performed in air. Measurements using our user facility Spectrolab XT-10 solar simulator were calibrated for 100 mW/cm^2 of AM 1.5 illumination using a reference Si solar cell. The response of the reference cell is periodically calibrated against a P3HT-based organic solar cell that has been submitted to the NREL Measurements and Characterization division for certified measurement. This provides an approximate correction for the spectral mismatch factor[29] but does not take into account day-to-day fluctuations in the lamp spectrum. Samples under test were loaded into a device holder with a quartz window. The lamp intensity for the XT-10 measurements was set such that the reflection off the top surface of the window, which is approximately 9%, was taken into account, and the intensity of light incident on the surface of the device was 100 mW/cm^2. Measurements using the XT-10 used a 395 nm high pass filter. Certified measurements performed by the NREL Measurements and Characterization division include a calculation of the spectral mismatch for each device measured. They do not take into account the reflection off the quartz window and do not use a 395 nm high pass filter. Current−voltage ($I-V$) measurements taken using a Keithley 238 high-current source power meter. External quantum efficiency (EQE) spectra were measured using a calibrated Si photodiode with a spot size smaller than the device area and intensity of 2 μW at 520 nm.

Results and Discussion

Growth and Characterization of ZnO Nanostructures. Nanofibers of ZnO were grown hydrothermally from solution with controlled fiber length, diameter, and orientation on a variety of substrates such as glass, quartz, sapphire, as well as

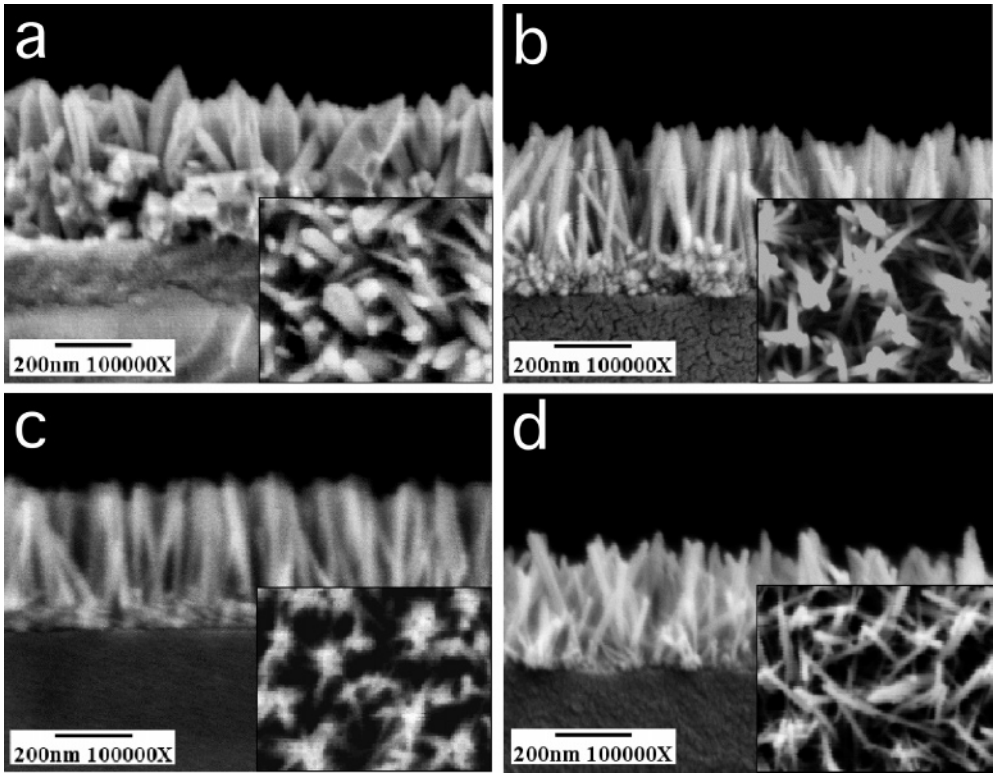

Figure 2. SEM images of ZnO fibers grown on annealed ZnAc nucleation layers spin-coated onto glass substrates. Nucleation layers are annealed at (a) 500 °C for 60 min, (b) 300 °C for 30 min, (c) 240 °C for 10 min, and (d) 300 °C for 5 min.

ITO, and F:SnO_2. Nanofibers grow only off of a previously deposited ZnO nucleation layer formed by annealing a spin-coated ZnAc layer. The morphology of these nanostructured oxide films was characterized by SEM in both plan view and in cross section. The factors affecting fiber length are the growth time, temperature, concentration, and pH. In general, the fiber diameter is determined by the structure of the nucleation layer from which the fibers are grown. The ZnO nucleation layer is spin-coated from a ZnAc solution and subsequently annealed in air to form a ZnO film. The diameter of the ZnO fibers is closely related to the temperature at which the ZnAc film is annealed. Figure 2 demonstrates that fibers grown off of a nucleation layer formed at 500 °C (Figure 2a) have a significantly larger diameter than those formed at 300 °C (Figure 2b) or at 240 °C (Figure 2c). The fiber orientation can be controlled by the anneal time of the nucleation layer. Growth on a nucleation layer annealed at 300 °C for 30 min (Figure 2b) shows well-aligned nanofibers, whereas fibers grown off of a nucleation layer annealed at 300 °C for 5 min result in more disordered fiber orientation. The disordered fiber growth is likely due in part to a reduced number of nucleation sites for fiber growth as well as the disordered fibers leading to the obstruction of dense fiber growth and incomplete fiber nucleation (Figure 2d).

Fourier tranform IR spectra of the ZnO films derived from ZnAc suggested that the organic was fully dissociated during the 300 °C anneal and confirmed that the fibers grown off of the nucleation layer are ZnO.

XRD characterization indicates that both the nucleation layer and the fibers are ZnO with the wurzite crystal structure, and that the crystalline nanofibers grow preferentially in the (002) direction, as seen in Figure 3. The nucleation layers in the films used to obtain the data in Figure 3 were annealed for 5 min at 300 °C, and as discussed above there was no texturing or preferred orientation for the grains grown from the substrate, which resulted in disordered fiber growth.

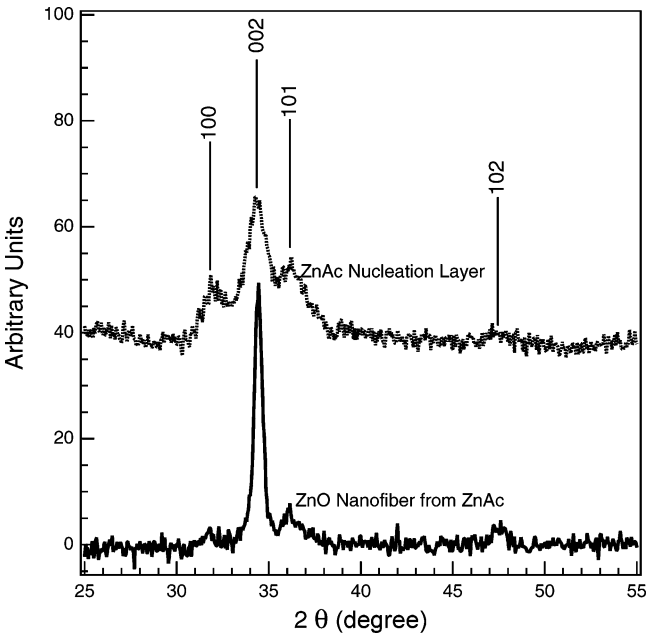

Figure 3. XRD data for annealed ZnAc nucleation layer (top) and ZnO nanofiber film (bottom). ZnO fibers were grown at pH 12, 70 °C for 20 min from a ZnAc nucleation layer annealed at 300 °C for 5 min.

The defect structure of the ZnO films was investigated by PL at an excitation wavelength of 275 nm. As shown in Figure 4, the PL emission spectrum for the ZnO nucleation layer differs slightly from that of the ZnO fibers. The visible emission from the ZnO nucleation layer is red-shifted and is of lower relative intensity compared to the band edge emission. The feature at 430 nm is attributed to an artifact, as it is observed in the PL

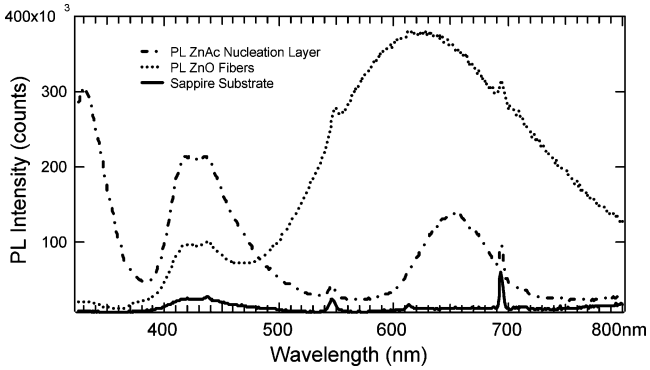

Figure 4. PL spectra of ZnO fibers (dot), ZnO nucleation layer (dash-dot), and sapphire substrate (solid line). ZnAc layer annealed at 300 °C for 30 min, and ZnO fibers grown at pH 12, 70 °C for 20 min.

spectrum from the sapphire substrate. The ZnO fibers have a much higher relative intensity for the visible emission and as a result might have a larger number of surface defect states than the ZnO nucleation layer. The decreased relative intensity of the band edge emission indicates an increase in the number of surface defect states as observed previously by other groups looking at the size dependence of the PL on ZnO fibers.[30] This may be important in device performance, as a higher number of surface defects in the ZnO could result in increased recombination. The defect-related emission located at 625−650 nm is often associated with oxygen defects such as interstitials in the ZnO structure.[31] To reduce the relative intensity of the visible emission, the ZnO fibers can be annealed in a variety of reducing environments, leading to improved band edge emission.[32] Studies are in progress to observe the effects of such annealing treatments on the device performance.

Polymer Intercalation. Using the ZnO nanofibers grown on a glass/ITO substrate that is subsequently filled with P3HT, we were able to successfully fabricate devices that are very similar in structure to the cartoon shown in Figure 1. Figure 5 depicts the ZnO nanocarpet structures after intercalation with P3HT. As shown, the polymer can be intercalated into the ZnO fiber film thus making a hybrid nanostructured oxide/conjugated polymer composite device. The nanostructured device in Figure 5a does not demonstrate complete intercalation of the polymer into the ZnO pore structure. Nonetheless, functioning photovoltaic devices with good device performance were fabricated using this structure. The use of various wetting agents, such as chlorosilanes (through soaking in a dry 5% phenyltrichlorosilane solution in toluene followed by a toluene rinse), enhanced the degree of intercalation substantially, as shown in Figure 5b. To date, however, these treatments have resulted in reduced photovoltaic performance than without their use. The phenyltrichlorosilane blocked the electron-transfer process at the polymer−oxide interface without any apparent effects on charge transport. The phenyltrichlorosilane appears to be acting as an insulator at the interface, which does not allow for electron transfer from the polymer to the ZnO. As such, the devices presented do not use any wetting treatment. Further studies of the topic are currently underway.

Effect of Processing Atmosphere on Device Performance. The photovoltaic performance of the polymer/ZnO nanofiber devices was observed to be dependent on the processing conditions and environments for this study. The P3HT/ZnO nanofiber devices were deposited onto a patterned ITO transparent coated with a ZnAc nucleation layer annealed at 300 °C for 5 min. ZnO fibers were then grown to a length of about 400 nm, rinsed, and dried at 200 °C for 30 min in air. The P3HT

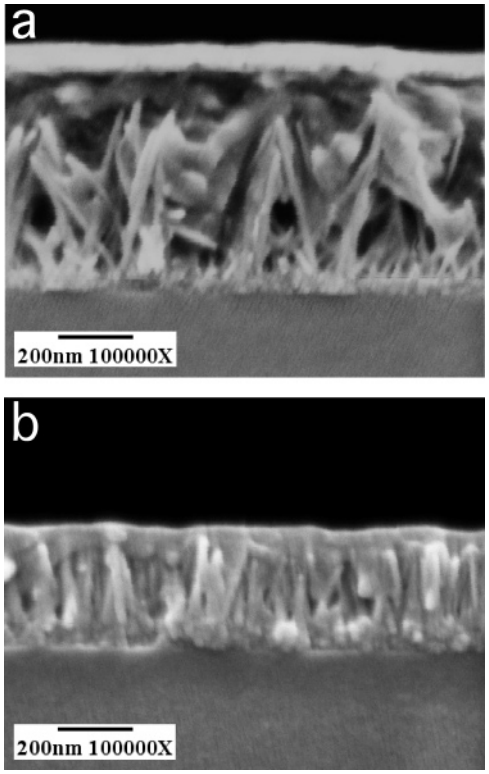

Figure 5. (a) Cross sectional SEM image of ZnO fiber/P3HT device without complete intercalation of polymer. (b) SEM image of P3HT completely intercalated into the nanocarpet structure treated with phenyltrichlorosilane.

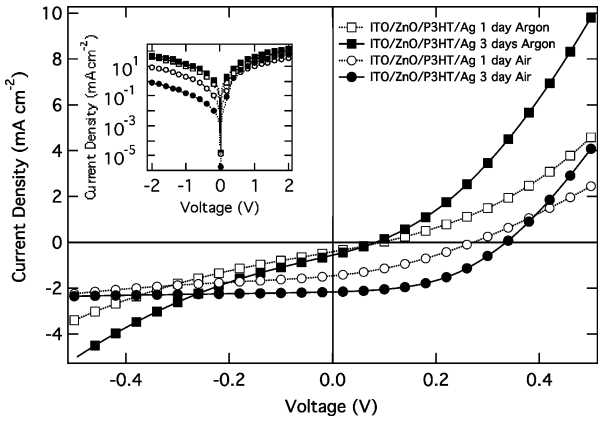

Figure 6. Current density versus voltage ($J-V$) for illuminated ITO/ZnO/ZnO fibers/P3HT/Ag devices aged in argon and air. Aging in argon 1 day (open square), argon 3 days (solid square), air 1 day (open circle), and air 3 days (solid circle). Inset shows dark $J-V$ curves.

layer was spin-coated at 800 RPM from a 30 g/L P3HT solution in chloroform in argon. The polymer film was then annealed at 200 °C for 1 min followed by a 5 min anneal at 120 °C in the glove box. Finally, the Ag electrode was evaporated, and the devices were characterized in argon. When the nanofiber devices were characterized through the measurement of $J-V$ curves under illumination and without exposure to air, they were shorted with little diode effect.

Storing the separate devices in the dark in argon and air for 24 h caused the performance of the device stored under argon to decrease, whereas the performance of the device stored under air increased, as seen in Figure 6. This is similar to observations from bilayer hybrid devices where aging in air improved device performance.[33] After 3 days in argon, the device continued to decrease in performance. The performance of the device stored

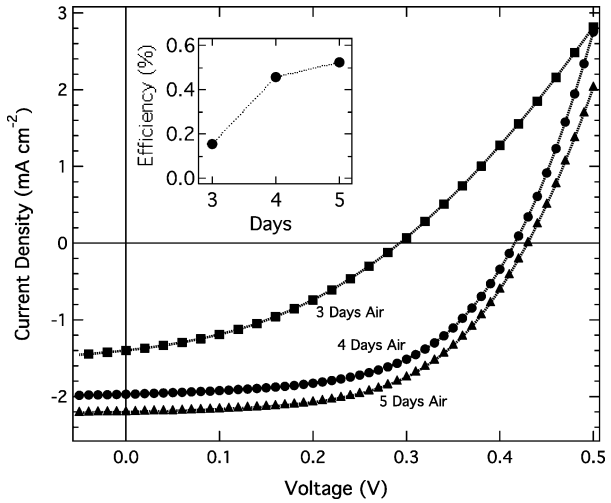

Figure 7. Current density versus voltage ($J-V$) for illuminated ITO/ZnO/ZnO fibers/P3HT/Ag device aged in air for 3 days (square), 4 days (circle), and 5 days (triangle). Inset shows device efficiency versus aging time in air.

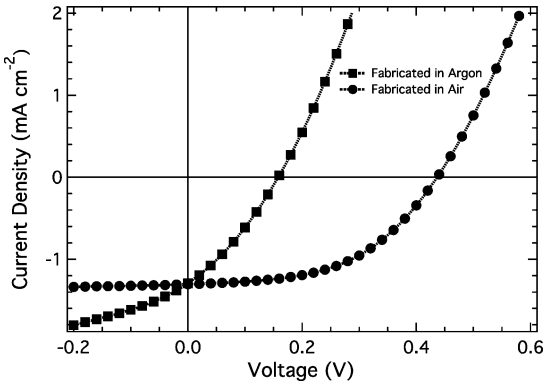

Figure 8. Current density versus voltage ($J-V$) for illuminated ITO/ZnO/ZnO fibers/P3HT/Ag devices spin-coated in argon in (square) and in air (circle).

in air for 3 days, however, increased substantially. The $J-V$ curves in Figure 6 indicate that the performance of the device stored in air increases through both an increase in the shunt resistance and a decrease in the series resistance, leading to increased FF and V_{OC} values. Hybrid polymer/metal oxide device sensitivity to atmosphere has been observed in similar systems based on a different polymer material and various metal oxides.[33−35] It is well known that oxygen vacancies are intrinsic electron donors in ZnO.[36,37] These vacancies may be quenched when stored in air or pure oxygen, and the semiconductor properties improve as both the oxygen vacancy and carrier concentrations are reduced. Devices stored in argon increase in oxygen vacancy density,[35] which increases the carrier density in the ZnO nanofibers and reduces the device performance. This agrees with the reduction of the series resistance, and a decrease in the shunt resistance in the $J-V$ curves. When the ZnO nanofibers were annealed at 300 °C for 1 h prior to the spin-coating the polymer film, the behavior was similar to the 200 °C drying step used in the presented data. However, the PL data presented above do not support this argument because the energy of the defect in the visible part of the spectra is not consistent with oxygen vacancies.

When the polymer/ZnO nanofiber device was stored in air for longer periods of time, the performance increases dramatically. This is shown in Figure 7 for a single device measured after 3, 4, and 5 days. It was found that the aging process could be accelerated by thermally annealing the devices for various times and at various temperatures in air. Although the annealed devices improved from their as-deposited performance, they did not demonstrate improved performance over the devices aged at room temperature for 5 days.

To determine if the improvements seen with aging were due to oxidation of the silver contact, devices were fabricated with both silver and gold counter electrodes. The Au electrode is not expected to react significantly with oxygen, whereas Ag may form silver oxide. However, both the devices with Ag and Au demonstrate identical aging behavior when exposed to air. In addition, P3HT can be doped by oxygen.[38,39] This could enhance charge separation through the formation of a p−n junction with ZnO. However, devices prepared with either P3HT or poly[2-methoxy-5-(3′,7′-dimethyloctyloxy)-1,4-phenylene vinylene] (MDMO−PPV) demonstrate the same increased efficiency with aging in air. These results indicate that the effect is not related to the choice of electrode or doping of P3HT.

Recently, a similar trend has been observed in highly resistive ZnO. After exposure to vacuum, the resistivity of the ZnO decreases by more than an order of magnitude. To explain this, a conducting channel has been suggested to form at the ZnO surface.[40,41] This conductive channel has been observed at moderate vacuum levels at room temperature on the surface of bulk ZnO.[41] Upon exposure to air, the resistivity is reversibly increased over several hours. Because of the enhanced surface area of the ZnO nanofiber material, the susceptibility may very well be increased in these devices.

On the basis of these observations, devices were fabricated by spin-coating the polymer film onto the ZnO nanofiber film in air outside of the glove box. The devices fabricated in air demonstrated higher performance, as seen in Figure 8 for typical devices prepared in air and in argon. As a result, all of the devices presented subsequently have been fabricated, stored, and characterized in air unless otherwise noted.

Effect of ZnO Nanofiber Orientation and Length on Device Performance. To decrease the fiber spacing, the ZnAc nucleation layer can be annealed for 30 min, which results in higher density, vertically oriented ZnO nanofibers as seen in Figure 2b. The increase in the fiber density should be reflected in an increase in the interfacial area of the heterojunction, which should increase the J_{SC} and lower the series resistance in the device. It was found that, despite having a higher density of ZnO fibers, devices made with vertical fibers demonstrated reduced performance as seen in Figure 9. The V_{OC} is reduced more dramatically than the J_{SC} perhaps as a result of reduced surface state passivation by the intercalation of the polymer into the ZnO nanofiber film. This is believed to be the result of poorer wetting by the P3HT in the case of more ordered fibers grown. Poorer wetting of the polymer can be explained by the polarity of the ZnO fiber surfaces, as it is known that the top (001) surface of the ZnO fiber is polar, whereas the side (100) surfaces are nonpolar.[42] We have observed that when the polymer is presented with a disordered film of nanofibers it wets much better than a closely packed array of fibers where the polymer might only come into contact with the top surface.

Another way to improve performance involves modifying the ZnO nanofiber length to optimize the active layer thickness. In this study, devices were fabricated with ZnO nanofiber lengths of about 500 and 250 nm by decreasing the growth time from 20 to 10 min, respectively. These polymer/ZnO nanofiber devices increase in efficiency as the active layer thickness increases up to 500 nm, as seen in Figure 10. The J_{SC} increases

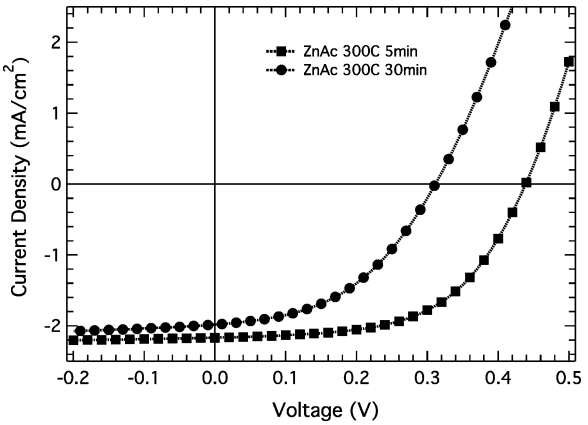

Figure 9. Current density versus voltage ($J-V$) for illuminated ITO/ZnO/ZnO fibers/P3HT/Ag with ZnO fibers grown for 20 min and ZnAc nucleation layer annealed at 300 °C for 5 min (square) and for 30 min (circle).

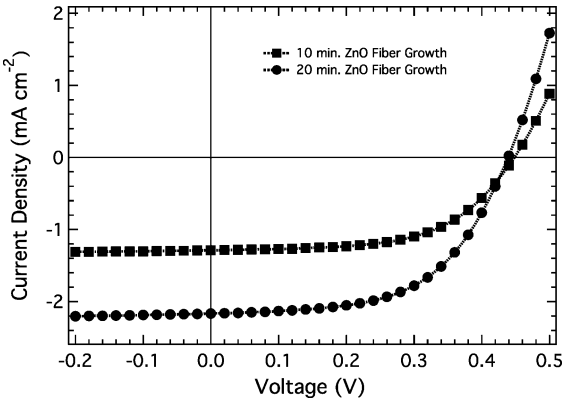

Figure 10. Current density versus voltage ($J-V$) for illuminated ITO/ZnO/ZnO fibers/P3HT/Ag with ZnAc nucleation layer annealed at 300 °C for 5 min and ZnO nanofibers grown for 10 min (squares) and for 20 min (circles).

from 1.29 mA cm^{-2} for the device with 250 nm ZnO nanofibers to 2.17 mA cm^{-2} for the 500 nm ZnO nanofiber device.

The J_{SC} increases despite the increased distance required for both holes and electrons to travel out of the device. This is not a general observation for ordered polymer/inorganic devices. In fact, for devices based on P3HT and mesoporous TiO_2 the opposite was observed at very low optical densities.[19] Efficient charge transport out of the P3HT/ZnO nanofiber device could be related in part to the increased electron mobility in the ZnO nanofibers. However, the hole mobility of the polymer is equally important in the device performance. Therefore, increasing the hole mobility of the polymer should lead to increased device performance. An alignment of the P3HT chain vertically along the ZnO nanofiber surface could lead to such an enhancement. This will be discussed in more detail below.

Photovoltaic Performance of ZnO Bilayer versus ZnO Nanofiber Devices. To observe the effect of the nanostructured oxide interface on the photovoltaic device performance, the nanostructured hybrid device was compared to a planar, bilayer device. The photovoltaic performance of the devices was characterized under simulated AM 1.5 illumination using a Spectrolab XT-10 solar simulator with an intensity of 100 mW/cm^2. The measurement was made with a 395 nm high pass UV filter inserted in front of the device to prevent photoexcitation of the ZnO. $J-V$ curves for both the bilayer and nanofiber ZnO devices are shown in Figure 11. The bilayer device of P3HT on the planar ZnO nucleation layer exhibited a V_{OC} of 500 mV, J_{SC} of 0.52 mA/cm^2, *FF* of 55%, and η of 0.15%. The performance of the nanostructured hybrid device was significantly improved with values for the V_{OC}, J_{SC}, *FF*, and η of 440 mV, 2.17 mA/cm^2, 56%, and 0.53%, respectively. This represents more than a 3-fold increase in power conversion efficiency, which is largely related to the increase in J_{SC}. A higher J_{SC} is expected as a result of increased interfacial area of the heterojunction between the ZnO and the P3HT.

The performance is improved compared to previous attempts by other groups using nanostructured TiO_2, where J_{SC} values were much smaller.[19,20] To verify the efficiency of the nanostructured device, the nanostructured device was submitted to the NREL Measurements and Characterization division for certified measurement, and the results are shown in the inset to Figure 11. These measurements do not take into account reflections off the face of a quartz window in our sample holder, which reflects approximately 9% of the incident light and does not use a UV filter to prevent photoexcitation of the ZnO. The results yield values for the V_{OC}, J_{SC}, *FF*, and η of 429 mV, 2.13 mA/cm^2, 48.4%, and 0.44%, respectively.

The certified measurement was performed without a UV filter, and the decreases in the V_{OC} and *FF* in the certified measurement are attributed to photoexcitation of the ZnO, which destabilizes the device. The destabilization of the device performance under UV illumination in organic and hybrid photovoltaic devices has been observed in other systems as well.[33,43] While the exact nature of this destabilization is unclear, a possible explanation is that photoexcitation of the ZnO leads to an increase of the defect density on the surface of the ZnO that acts to increase carrier recombination at the ZnO/P3HT interface. These changes are reversible, however. Leaving the device in the air in the dark for several hours restores the original V_{OC} and *FF* prior to UV exposure. Therefore, photooxidation of the P3HT at the ZnO surface is not a reasonable explanation, because this would lead to permanent changes in device performance. Interestingly, the ZnO/P3HT bilayer devices do not show this large sensitivity to UV exposure. This may be a result of the decreased surface area of the ZnO/P3HT interface, or the surface chemistries of the ZnO derived from a ZnAc precursor in the nucleation layer as opposed to the zinc nitrate precursor used in the nanofibers.

The EQE spectra for both the bilayer ITO/ZnO/P3HT/Ag and the nanostructured ITO/ZnO fibers/P3HT/Ag devices were measured and compared to the absorption spectrum for a corresponding nanostructured composite film, as seen in Figure 12. The relatively low EQE values for both devices indicate that much of the light absorbed is not converted to charge carriers, which is likely due to the large spacing between fibers (100 nm) and the short exciton diffusion length found in P3HT (3−5 nm).[44] The bilayer device produced a maximum EQE of 6.2% at 510 nm, corresponding to a J_{SC} of 0.52 mA/cm^2. The nanostructured ZnO fiber device achieved a maximum EQE of 18.3% at 520 nm corresponding to 2.1 mA/cm^2. The peak in both EQE spectra at 360 nm is the result of UV light absorption by the ZnO and subsequent hole transfer to the P3HT. This demonstrates that there are contributions to the photocurrent from light absorption in both P3HT and ZnO. Integration of the measured spectral response of the nanostructured device with the AM 1.5 solar spectrum (100 mW/cm^2) results in an estimated J_{SC} of 2.06 mA/cm^2, which agrees very well with the observed white light J_{SC} above. The normalized EQE spectra of both devices indicate that there is a small red shift in the photoresponse of the nanostructured device, as seen in the inset in Figure 12. This red shift in the EQE of polymer/ZnO nanofiber device could be due to increased molecular order of the P3HT chains along the vertical surface of the nanofibers.

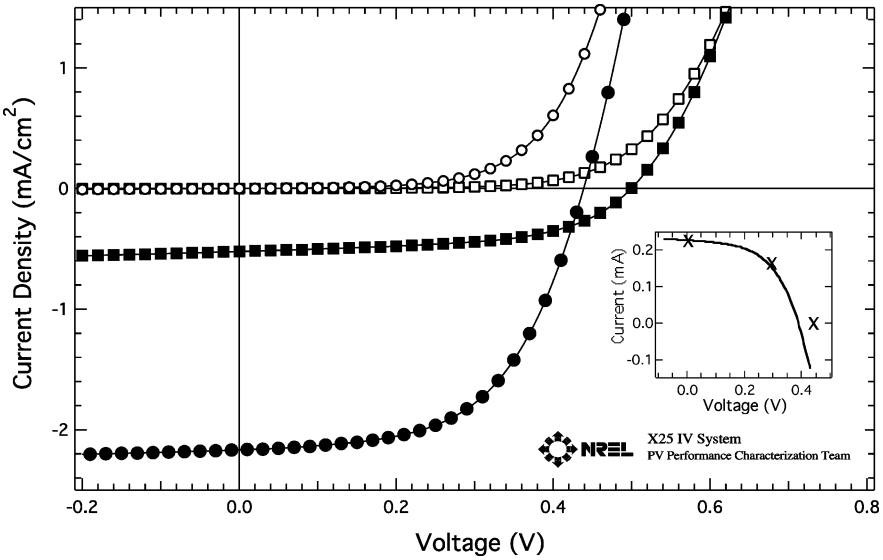

Figure 11. Current density versus voltage ($J-V$) for a typical ITO/ZnO/P3HT/Ag bilayer device (solid squares) and ITO/ZnO fiber/P3HT/Ag device (solid circles) under AM 1.5 illumination and in dark (open squares) and (open circles), respectively. The light intensity is corrected by the spectral mismatch factor of 100 mW/cm^2. Inset shows NREL certified measurement data.

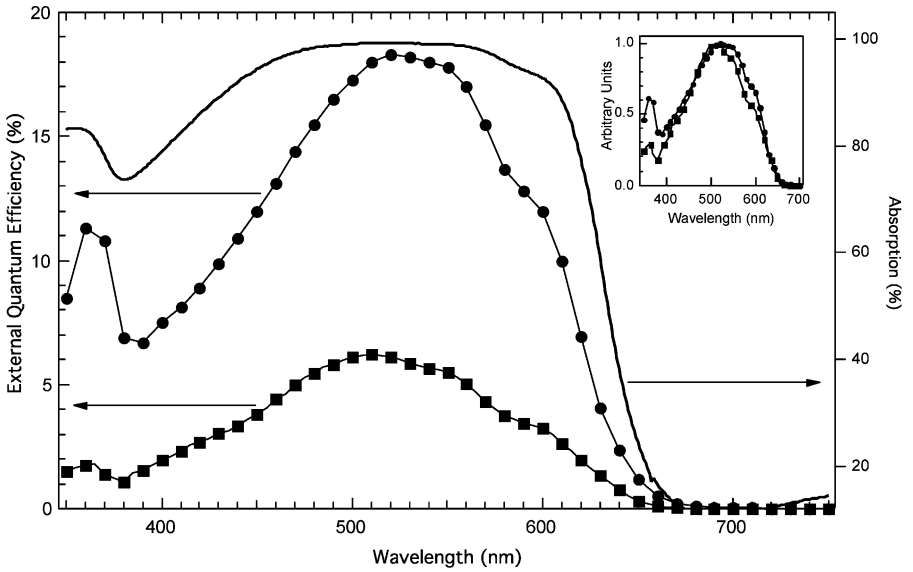

Figure 12. External quantum efficiency of ITO/ZnO/P3HT/Ag bilayer device (squares), ITO/ZnO fibers/P3HT/Ag nanostructured device (circles) and UV−vis absorption spectrum of the nanostructured device (solid line). Inset shows normalized spectra.

There are several possible routes to improving the performance of the nanostructured devices. The V_{OC} is lower than expected from this donor−acceptor pair. Bulk heterojunction devices using a common donor polymer such as MDMO−PPV blended with PCBM as an acceptor have demonstrated similar V_{OC} values to hybrid blend devices using ZnO nanoparticles.[11,45,46] Devices consisting of blends of P3HT and PCBM have yielded a V_{OC} of approximately 600 mV, and therefore a similar V_{OC} might be expected in these devices. The reason the V_{OC} seen in the device is substantially lower than this is not clear, but possible explanations include the presence of midgap states on the surface of the ZnO that pin the Fermi level, or that the electron mobility of the ZnO nanofibers could actually be too high, resulting in increased carrier recombination at the ZnO/P3HT interface and a reduced V_{OC}. Further studies are necessary to better understand these phenomena.

The spacing between the disorded ZnO nanofibers is about 100 nm in the devices presented here. This is much larger than the exciton diffusion length for P3HT, which is estimated to be less than 5 nm.[44] However, we do not know how ordering of the P3HT chains inside the pores of the ZnO may affect either the exciton diffusion length or the hole mobility. Recently, it has been observed that P3HT incorporated into small vertically oriented pores in anodic alumina can lead to improved hole mobility in the polymer.[47,48] The hole mobility was observed to increase from 3×10^{-4} to 6×10^{-3} cm^2 V^{-1} s^{-1} in the charge transport direction.[48] The P3HT chains were observed to be partially aligned along the side of the vertically oriented poses in the anodic alumina film. Given that the charge transport direction in the photovoltaic device is normal to the substrate, this is encouraging for this polymer/nanofiber device configuration. Additionally, if the polymer chains increase in order from the middle of the pore to the nanofiber surface, then the exciton diffusion will be directed toward the dissociation interface because of the downward gradient in band gap energies of the exciton transport sites. This suggests that closer spacing of the fibers should yield a larger J_{SC} and thereby increase the efficiency.

Dependence of Photovoltaic Performance on Light Intensity. Additional, $J-V$ measurements were taken at light intensi-

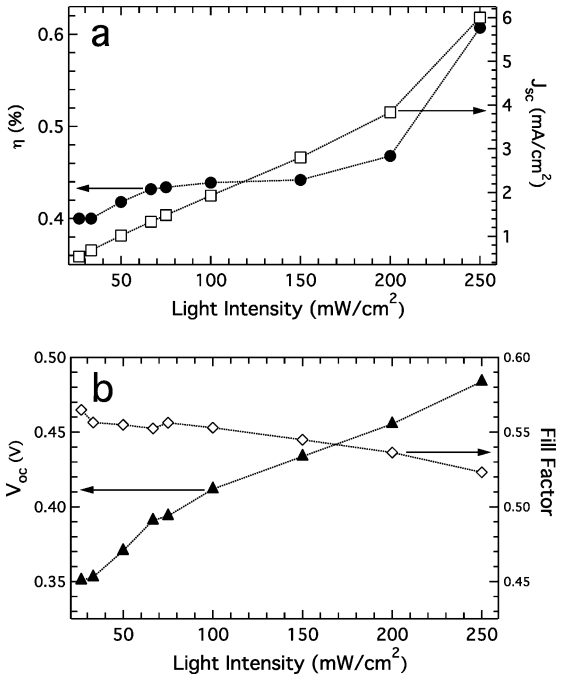

Figure 13. PV performance vs illumination intensity of the nanostuctured hybrid device. Power conversion efficiency and short circuit current vs intensity (a), open circuit voltage and fill factor vs intensity (b). Intensity varied by changing distance from the lamp using Spectrolab XT-10 solar simulator (AM 1.5).

ties ranging from 0.25 suns (25 mW/cm^2) to 2.5 suns (250 mW/cm^2) as seen in Figure 13. In this typical device, the data indicate that the efficiency increased from 0.40 to 0.61% at 0.25 and 2.5 suns, respectively. The short circuit current density increases linearly with intensity up to 200 mW/cm^2 ($J_{SC} \propto I^{\sim 1}$), indicating that charge carrier losses are dominated by monomolecular recombination. However, above 200 mW/cm^2 the relationship between J_{SC} and intensity becomes super linear. The increase in V_{OC} is greater than the logarithmic relationship that is anticipated. These observations might be explained through increased trap filling in the ZnO at higher light intensities. The direction of the measurements was from low to high intensity; the same observations were seen in measurements made from high to low intensity. Increased efficiencies at higher light intensities have been demonstrated in small molecule-based photovoltaic devices when the series resistance is carefully minimized.[49] However, this observation is rare for polymer photovoltaic devices, which typically exhibit their best efficiency at or below intensities of 1 sun (100 mW/cm^2), indicating a possible advantage in this hybrid device architecture.

Effect of Interface Modifiers on Bilayer Photovoltaic Performance. A surface modifier was employed in hopes of improving both the polymer intercalation into the ZnO nanofiber film and the photovoltage to the expected value. Enhanced performance in organic light−emitting diodes has been observed using nonionic polyethylene glycol either blended into the electroluminescent layer (EL) or at the interface between the EL and the cathode.[50,51] Polyoxyethylene(12) tridecyl ether (P_{12}-TE) was dissolved in methanol at a concentration of 5 g/L. A thin (<10 nm) P_{12}TE film was formed by spin-coating the solution at 4 000 rpm onto the ZnO film prior to polymer deposition. The effect of the P_{12}TE pretreatment on P3HT/ZnO bilayer devices was significant. The V_{OC} increased dramatically from 401 to 683 mV for a bilayer device treated with P_{12}TE, as seen in Figure 14. However, the J_{SC} is reduced from 0.78 mA to 0.36 mA cm^{-2}.

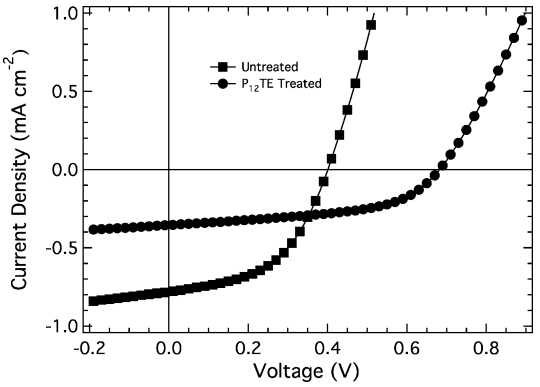

Figure 14. Current density versus voltage for typical ITO/ZnO/P3HT/Ag device (squares) and ITO/ZnO/P_{12}TE/P3HT/Ag device (red circles).

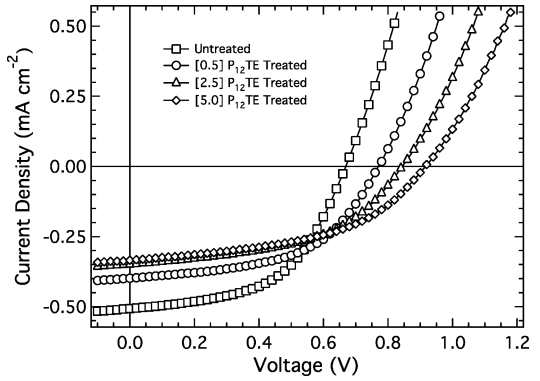

Figure 15. Current density versus voltage for typical ITO/ZnO/PPV/Ag device (squares), ITO/ZnO/[0.5] P_{12}TE/PPV/Ag device (circles), ITO/ZnO/[2.5] P_{12}TE/PPV/Ag device (triangles), and ITO/ZnO/[5.0] P_{12}TE/PPV/Ag device (diamonds).

To observe the effect of P_{12}TE thickness on device performance, devices using lower concentration P_{12}TE solutions were fabricated. In addition, to see if the effect was selective to the polymer itself, bilayer MDMO−PPV/ZnO bilayer devices were fabricated. Increasing concentration of P_{12}TE from the untreated device to pretreatment with a 0.5, 2.5, and 5 g/L leads to a systematic increase in V_{OC} with a systematic reduction in the J_{SC} with P_{12}TE coverage, as seen in Figure 15. Again, this could be due to increased thickness as an insulator with increased concentration or to the increase in coverage with increased concentration. Further investigation is needed to determine the mechanism for increased V_{OC}. Additionally, the effect is not unique to the P3HT/ZnO system, as demonstrated in the PPV/ZnO devices.

The effect of P_{12}TE treatment on ZnO nanofiber devices was similar to the bilayer devices; however, the relative changes were much smaller. Devices pretreated with P_{12}TE demonstrated higher V_{OC} values. The increase in V_{OC} in the ZnO nanofiber device was great enough to offset the decreased J_{SC} and lead to power conversion efficiencies equal to that of the untreated annealed nanofiber device above. This could be attributed to either the addition of an insulating layer between the donor and acceptor pair or the result of a surface dipole to create a vacuum level offset between donor and acceptor leading to an alteration of the V_{OC} in the device.[52]

Conclusions

We have demonstrated aqueous solution growth of ZnO nanostructures that are vertically aligned off of the substrate.

Present results from PV devices made with ZnO nanofibers/P3HT composite structures have yielded an efficiency of 0.53% under AM 1.5 illumination, which is significantly greater than that of a similar bilayer structure. An increased efficiency to 0.61% was observed at higher light intensities, indicating the possible advantage in using high-mobility electron transport pathways. The present devices need to be fabricated in and exposed to air to ensure proper device operation. Disordered ZnO nanofibers resulted in higher device performance despite having lower density and higher fiber spacing. The surface treatment explored here had little effect overall on device efficiency due to the reduced J_{SC} that compensates for the higher observed V_{OC} values. While these efficiencies are still lower than other hybrid organic photovoltaic devices, there are clear limitations in the current device architecture. Several paths are being pursued that might lead to higher efficiencies. The inverted device architecture allows for device fabrication and storage in air, which is prohibited in the majority of organic photovoltaic devices. Work is underway to understand and improve the performance of this device structure.

Acknowledgment. The authors gratefully acknowledge the many fruitful discussions with Professor Mike McGehee and Yuxiang Liu at Stanford University, Professor Clark Fields and Rene Peterson at the University of Northern Colorado, and Dr. Brian Gregg, Dr. Garry Rumbles, and Matthew White at NREL. The authors also thank Bobby To at NREL for the production of SEM images, Iain McCulloch at Merck for providing P3HT, and financial support for research in organic photovoltaics through the NREL DDRD program and DARPA. Work at NREL is supported by the U.S. DOE under Contract No. DE-AC36-99GO10337.

References and Notes

(1) Shaheen, S. E.; Ginley, D. S.; Jabbour, G. E. *MRS Bull.* **2005**, *30*, 10.

(2) Brabec, C. J.; Hauch, J.; Choulis, S.; Schilinsky, P.; Zeira, E.; Sokolik, I. Challenges in Flexible Organic Phovoltaics. In *Organic and Nanoparticle Hybrid Photovoltaic Devices*; MRS Spring Meeting, San Francisco, April 10, 2007; Materials Research Society: San Francisco, CA, 2007.

(3) Green, M. A.; Emery, K.; Hisikawa, Y.; Warta, W. *Prog. Photovoltaics* **2007**, *15*, 425.

(4) Note added in proof: Dennler, G.; Forberich, K.; Scharber, M. C.; Brabec, C. J.; Hingerl, K.; Fromherz, T. Optical considerations in bulk-heterojunction solar cells; SPIE Optics + Photonics, San Diego, CA, August 29, 2007.

(5) Brabec, C. J. *Sol. Energy Mater. Sol. Cells* **2004**, *83*, 273.

(6) Padinger, F.; Rittberger, R. S.; Sariciftci, N. S. *Adv. Funct. Mater.* **2003**, *13*, 85.

(7) Savenije, T. J.; Warman, J. M.; Goossens, A. *Chem. Phys. Lett.* **1998**, *287*, 148.

(8) Arango, A. C.; Johnson, L. R.; Bliznyuk, V. N.; Schlesinger, Z.; Carter, S. A.; Hörhold, H.-H. *Adv. Mater.* **2000**, *12*, 1689.

(9) van Hal, P. A.; Wienk, M. M.; Kroon, J. M.; Verhees, W. J. H.; Slooff, L. H.; van Gennip, W. J. H.; Jonkheijm, P.; Janssen, R. A. J. *Adv. Mater.* **2003**, *15*, 118.

(10) Salafsky, J. S. *Phys. Rev. B* **1999**, *59*, 10885.

(11) Beek, W. J. E.; Wienk, M. M.; Janssen, R. A. J. *Adv. Mater.* **2004**, *16*, 1009.

(12) Beek, W. J. E.; Slooff, L. H.; Wienk, M. M.; Kroon, J. M.; Janssen, R. A. J. *Adv. Funct. Mater.* **2005**, *15*, 1703.

(13) Huynh, W. U.; Dittmer, J. J.; Alivisatos, A. P. *Science* **2002**, *295*, 2425.

(14) Ginger, D. S.; Greenham, N. C. *Synth. Met.* **2001**, *124*, 117.

(15) Olson, D. C.; Piris, J.; Collins, R. T.; Shaheen, S. E.; Ginley, D. S. *Thin Solid Films* **2006**, *496*, 26.

(16) Peiró, A. M.; Ravirajan, P.; Govender, K.; Boyle, D. S.; O'Brien, P.; Bradley, D. D. C.; Nelson, J.; Durrant, J. R. *J. Mater. Chem.* **2006**, *16*, 2088.

(17) Ravirajan, P.; Peiro, A. M.; Nazeeruddin, M. K.; Graetzel, M.; Bradley, D. D. C.; Durrant, J. R.; Nelson, J. *J. Phys. Chem. B* **2006**, *110*, 7635.

(18) Coakley, K. M.; Liu, Y.; McGehee, M. D.; Frindell, K. L.; Stucky, G. D. *Adv. Funct. Mater.* **2003**, *13*, 301.

(19) Coakley, K. M.; McGehee, M. D. *Appl. Phys. Lett.* **2003**, *83*, 3380.

(20) Ravirajan, P.; Haque, S. A.; Durrant, J. R.; Bradley, D. D. C.; Nelson, J. *Adv. Funct. Mater.* **2005**, *15*, 609.

(21) Kaidashev, E. M.; Lorenz, M.; Wenckstern, H. v.; Rahm, A.; Semmelhack, H.-C.; Han, K.-H.; Benndorf, G.; Bundesmann, C.; Hochmuth, H.; Grundmann, M. *Appl. Phys. Lett.* **2003**, *82*, 3901.

(22) Makino, T.; Segawa, Y.; Tsukazaki, A.; Ohtomo, A.; Kawasaki, M. *Appl. Phys. Lett.* **2005**, *87*, 022101.

(23) Konenkamp, R.; Boedecker, K.; Lux-Steiner, M. C.; Poschenrieder, M.; Zenia, F.; Levy-Clement, C.; Wagner, S. *Appl. Phys. Lett.* **2000**, *77*, 2575.

(24) Law, M.; Greene, L. E.; Johnson, J. C.; Saykally, R.; Yang, P. *Nat. Mater.* **2005**, *4*, 455.

(25) Ohyama, M.; Kozuka, H.; Yoko, T. *Thin Solid Films* **1997**, *306*, 78.

(26) Vayssieres, L. *Adv. Mater.* **2003**, *15*, 464.

(27) Peterson, R. B.; Fields, C. L.; Gregg, B. *Langmuir* **2004**, *20*, 5114.

(28) Lachkar, A.; Selmani, A.; Sacher, E.; Leclerc, M.; Mokhliss, R. *Synth. Met.* **1994**, *66*, 209.

(29) Sommeling, P. M.; Rieffe, H. C.; Roosmalen, J. A. M. v.; Schönecher, A.; Kroon, J. M.; Wienke, J. A.; Hinsch, A. *Sol. Energy Mater. Sol. Cells* **2000**, *62*, 399.

(30) Shalish, I.; Temkin, H.; Narayanamurti, V. *Phys. Rev. B* **2004**, *69*, 245401.

(31) Cross, R. B. M.; Souza, M. M. D.; Narayanan, E. M. S. *Nanotechnology* **2005**, *16*, 2188.

(32) Greene, L. E.; Law, M.; Goldberger, J.; Kim, F.; Johnson, J. C.; Zhang, Y.; Saykally, R. J.; Yang, P. *Angew. Chem., Int. Ed.* **2003**, *42*, 3031.

(33) Lira-Cantu, M.; Norrman, K.; Andreasen, J. W.; Casan-Pastor, N.; Krebs, F. C. *J. Electochem. Soc.* **2007**, *154*, B508.

(34) Lira-Cantu, M.; Krebs, F. C. *Sol. Energy Mater. Sol. Cells* **2006**, *90*, 2076.

(35) Lira-Cantu, M.; Norrman, K.; Andreasen, J. W.; Krebs, F. C. *Chem. Mater.* **2006**, *18*, 5684.

(36) Kohan, A. F.; Ceder, G.; Morgan, D.; Van, de Walle, C. G. *Phys. Rev. B* **2000**, *61*, 15019.

(37) Mahan, G. D. *J. Appl. Phys.* **1983**, *54*, 3825.

(38) Ong, B.; Wu, Y.; Jiang, L.; Liu, P.; Murti, K. *Synth. Met.* **2004**, *142*, 49.

(39) Ong, B. S.; Wu, Y.; Liu, P.; Gardner, S. *J. Am. Chem. Soc.* **2004**, *126*, 3378.

(40) Schmidt, O.; Geis, A.; Kiesel, P.; Van, de Walle, C. G.; Johnson, N. M.; Bakin, A.; Waag, A.; Döhler, G. H. *Superlattices Microstruct.* **2006**, *39*, 8.

(41) Schmidt, O.; Kiesel, P.; Van, de Walle, C. G.; Johnson, N. M.; Nause, J.; Döhler, G. H. *Jpn. J. Appl. Phys.* **2005**, *44*, 7271.

(42) Vayssieres, L.; Keis, K.; Hagfeldt, A.; Lindquist, S.-E. *Chem. Mater.* **2001**, *13*, 4395.

(43) Katz, E. A.; Gevorgyan, S.; Orynbayev, M. S.; Krebs, F. C. *Eur. Phys. J. Appl. Phys.* **2006**, *36*, 307.

(44) Kroeze, J. E.; Savenije, T. J.; Vermeulen, M. J. W.; Warman, J. M. *J. Phys. Chem. B* **2003**, *107*, 7696.

(45) Shaheen, S. E.; Brabec, C. J.; Sariciftci, N. S.; Padinger, F.; Fromherz, T.; Hummelen, J. C. *Appl. Phys. Lett.* **2001**, *78*, 841.

(46) Beek, W. J. E.; Wienk, M. M.; Kemerink, M.; Yang, X.; Janssen, R. A. J. *J. Phys. Chem. B* **2005**, *109*, 9505.

(47) Coakley, K. M.; Liu, Y.; Goh, C.; McGehee, M. D. *MRS Bull.* **2005**, *30*, 37.

(48) Coakley, K. M.; Srinivasan, B. S.; Ziebarth, J. M.; Goh, C.; Liu, Y.; McGehee, M. D. *Adv. Funct. Mater.* **2005**, *15*, 1927.

(49) Xue, J.; Uchida, S.; Rand, B. P.; Forrest, S. R. *Appl. Phys. Lett.* **2004**, *84*, 3013.

(50) Deng, X. Y.; Lau, W. M.; Wong, K. Y.; Low, K. H.; Chow, H. F.; Cao, Y. *Appl. Phys. Lett.* **2004**, *84*, 3522.

(51) Niu, Y.-H.; Ma, H.; Xu, Q.; Jen, A. K.-Y. *Appl. Phys. Lett.* **2005**, *86*, 083504.

(52) Liu, Y.; Scully, S. R.; McGehee, M. D.; Liu, J.; Luscombe, C. K.; Frechet, J. M. J.; Shaheen, S. E.; Ginley, D. S. *J. Phys. Chem. B* **2006**, *110*, 3257.